ISSN: 0256-307X

# 中国物理快报
# Chinese Physics Letters

Volume 32 Number 11 November 2015

A Series Journal of the Chinese Physical Society
Distributed by IOP Publishing

Online: http://iopscience.iop.org/0256-307X
http://cpl.iphy.ac.cn

CHINESE PHYSICAL SOCIETY
IOP Publishing

CHIN. PHYS. LETT. Vol. 32, No. 11 (2015) 115202

# Parametric Instabilities of Parallel Propagating Circularly Polarized Alfvén Waves: One-Dimensional Hybrid Simulations *

HE Peng(何鹏)[1], GAO Xin-Liang(高新亮)[1**], LU Quan-Ming(陆全明)[1], ZHAO Jin-Song(赵金松)[2]
[1] *CAS Key Laboratory of Geospace Environment, Department of Geophysics and Planetary Science, University of Science and Technology of China, Hefei 230026*
[2] *Purple Mountain Observatory, Chinese Academy of Sciences, Nanjing 210008*

(Received 10 July 2015)

*By performing one-dimensional (1-D) hybrid simulations, we analyze in detail the parametric instabilities of the Alfvén waves with a spectrum in a low beta plasma. The parametric instabilities experience two stages. In the first stage, the density modes are excited and immediately couple with the pump Alfvén waves. In the second stage, each pump Alfvén wave decays into a density mode and a daughter Alfvén mode similar to the monochromatic cases. Furthermore, the proton velocity beam will also be formed after the saturation of the parametric instabilities. When the plasma beta is high, the parametric decay in the second stage will be strongly suppressed.*

*PACS:* 52.35.Mw, 94.05.Pt, 52.65.Ww DOI: 10.1088/0256-307X/32/11/115202

Alfvén waves are the exact solutions of the ideal incompressible magnetohydrodynamic (MHD) equations regardless of their amplitudes, and the intensity of their total magnetic fields is a constant.[1−4] However, since Galeev[5] pointed out in 1963 that a monochromatic circularly polarized Alfvén wave can decay into one forward propagating ion acoustic wave and one backward propagating daughter Alfvén wave,[5−10] numerous works have been devoted to investigate the parametric instabilities of Alfvén waves via both theoretical analysis and numerical simulations.[5−24] In the MHD frame, the parametric instabilities of a monochromatic Alfvén wave can be divided into three types.[13,16,18] The decay instability can occur in a low beta plasma and generates one forward propagating ion acoustic wave ($k_{\rm s}$) and one backward propagating daughter Alfvén wave ($k^- = k_0 - k_{\rm s}$).[5−8,16,18] The beat instability generates one forward propagating ion acoustic wave ($k_{\rm s}$) and two daughter Alfvén waves that propagate forward and backward, respectively ($k^\pm = k_0 \pm k_{\rm s}$).[16,18] Such an instability can occur in both low and high beta plasmas for a left-handed polarized Alfvén wave, while for a right-handed polarized Alfvén wave, the beat instability can only take place in a high beta plasma with the amplitude of the pump wave reaching a higher threshold value ($A > 2|\omega_0|(\beta - 1)$, where $A$ and $\omega_0$ represent the normalized amplitude and frequency of a pump wave, respectively).[16,18] The modulation instability occurs in a two-fluid plasma and generates one forward propagating ion acoustic wave ($k_{\rm s}$) and two forward propagating daughter Alfvén waves ($k^\pm = k_0 \pm k_{\rm s}$).[11−13] The modulation instability occurs in a low beta plasma for a left-handed polarized Alfvén wave and in a high beta plasma for a right-handed Alfvén wave.[11−13,18]

Recently with 1-D hybrid simulations, Araneda *et al.*,[21] Nariyuki *et al.*[25,26] and Kauffmann *et al.*[27] found that ion dynamics can restrain the growth of the parametric decay of a parallel propagating Alfvén wave and can promote the excitation of the modulation instability.[21,25−27] Further, with 2-D hybrid simulation models,[28−31] Matteini *et al.*[28] and Gao *et al.*[30] have reported that the perpendicular parametric decay can occur for a parallel propagating either linearly or left-hand polarized pump Alfvén wave in a low beta plasma. Although a monochromatic pump Alfvén wave is preferentially used in the above studies, the Alfvén waves in plasma usually exhibit a spectral structure.[32−36] Consequently with a 1-D hybrid simulation model for the spectrum of Alfvén waves, Nariyuki *et al.*[26] and Matteini *et al.*[37] have found that the modulation instability and ponderomotive effect of the magnetic field will dominate the dissipation of the pump Alfvén waves at an early time of the evolution. In this Letter, we analyze in detail the parametric instabilities of the Alfvén waves with a spectrum in a low beta plasma, which is observed to experience two stages.

Here a 1-D hybrid simulation model under period boundary condition is employed, where the ions are described as particles, while the electrons are treated as the massless fluid.[38−40] The hybrid simulation model not only can simulate the ion dynamics more accurately than the MHD simulation model, but also can save more computing time than the PIC simulation model. The basic equations solved in the hybrid simulations are listed as follows:

$$m_{\rm i}\frac{d\boldsymbol{v}_{\rm i}}{dt} = e(\boldsymbol{E} + \boldsymbol{v}_{\rm i}\times\boldsymbol{B}) - e\eta\boldsymbol{J},$$

$$0 = n_{\rm e}m_{\rm e}\frac{d\boldsymbol{V}_{\rm e}}{dt} = -en_{\rm e}(\boldsymbol{E} + \boldsymbol{V}_{\rm e}\times\boldsymbol{B}) - \nabla p_{\rm e} + en_{\rm e}\eta\boldsymbol{J},$$

$$\mu_0\boldsymbol{J} = \nabla\times\boldsymbol{B},\quad \frac{\partial\boldsymbol{B}}{\partial t} = -\nabla\times\boldsymbol{E},\quad \frac{p_{\rm e}}{n_{\rm e}^{\gamma}} = \text{const},$$

*Supported by the National Natural Science Foundation of China under Grant Nos 41331067, 41474125, 41274144, 41174124 and 41121003, the National Basic Research Program of China under Grant Nos 2013CBA01503 and 2012CB825602, and the Key Research Program of Chinese Academy of Sciences under Grant No KZZD-EW-01-4.
**Corresponding author. Email: gaoxl@mail.ustc.edu.cn

with the electric field $\boldsymbol{E}$, the magnetic field $\boldsymbol{B}$, the current density $\boldsymbol{J}$, the ion velocity $\boldsymbol{v}_{\rm i}$, the electron bulk velocity $\boldsymbol{V}_{\rm e}$, the pressure of electrons $p_{\rm e}$, and the number density $n_{\rm e}$ (charge neutrality $n_{\rm e} = n_{\rm i} = n$). Here $e$, $m_{\rm i}$ and $m_{\rm e}$ represent the charge unit, the masses of ion and electron, respectively; $\eta$ is the resistivity, which represents wave-particle effects due to high frequency plasma instabilities that involve the electron mass. The state equation of electrons is adiabatic, where $\gamma$ represents the adiabatic index.

The simulations are performed in $x$-axis parallel to the ambient magnetic field ($\boldsymbol{B}_0$), and all physical quantities depend only on one spatial coordinate $x$. Here the plasma density, magnetic field, and velocity are normalized by the initial uniform density $\rho_0$, background magnetic field intensity $B_0$, and background Alfvén velocity $v_{\rm A} = B_0/\sqrt{\mu_0\rho_0}$, respectively. The time and space are normalized by the reciprocal of proton cyclotron frequency $\varOmega_{\rm p}^{-1} = m_{\rm p}/e_{\rm p}B_0$ ($m_{\rm p}$ is the mass of proton, and $e_{\rm p}$ is the charge of proton) and proton inertial length $c/\omega_{\rm pp}$ ($c$ is the speed of light in a vacuum, and $\omega_{\rm pp}$ is the proton plasma frequency based on the proton number density $n_{\rm p}$), respectively.

The initial pump Alfvén waves are given as[26,37]

$$\delta\boldsymbol{B}_{\rm p} = \sum_{k_0=k_1}^{k_n} \delta B_{k_0}[\cos(k_0x-\omega_0t+\phi_{k_0})\hat{\boldsymbol{y}} + \sin(k_0x-\omega_0t+\phi_{k_0})\hat{\boldsymbol{z}}], \tag{1}$$

$$\delta\boldsymbol{u}_{\rm p} = \sum_{k_0=k_1}^{k_n} \delta u_{k_0}[\cos(k_0x-\omega_0t+\phi_{k_0})\hat{\boldsymbol{y}} + \sin(k_0x-\omega_0t+\phi_{k_0})\hat{\boldsymbol{z}}], \tag{2}$$

where $\delta\boldsymbol{B}_{\rm p}$ is the magnetic fluctuation and $\delta\boldsymbol{u}_{\rm p}$ is the associated transverse velocity. The initial phase $\phi_{k_0}$ is given randomly with a range $[0, 2\pi]$. By using Eqs. (1) and (2), the initial pump Alfvén waves are set to be a linear superposition of parallel propagating left-handed Alfvén waves, which have a spectrum structure. Each initial pump Alfvén wave with the wave number $k_0$ and frequency $\omega_0$ is given by employing the dispersion relation obtained from the Hall-MHD equations,[14] for left-handed Alfvén wave $\omega_0^2 = k_0^2(1-\omega_0)$ and Walen's relation,[25] $\delta u_{k_0} = -\delta B_{k_0}/(\omega_0/k_0)$.

The number of grid cells is $n_x = 600$, the size of grid cell is $\Delta x = 1.0c/\omega_{\rm pp}$, the time step is $\Delta t = 0.025\varOmega_{\rm p}^{-1}$, and the electron resistive length is set to be $L_{\rm r} = \eta/\mu_0V_{\rm A} = 0.02c/\omega_{\rm pp}$, which is useful in eliminating unwanted high frequency noise. For protons, 900 macroparticles are initially evenly distributed in every cell. The total magnetic field energy of the initial pump Alfvén waves is set to be $\sum_{k_0=k_1}^{k_n}(\delta B_{k_0}/B_0)^2 = 0.04$, and the amplitude of each initial pump Alfvén wave is equal.

Three simulation runs are performed. The electron beta $\beta_{\rm e}$, the proton beta $\beta_{\rm p}$, and the wave numbers of the initial pump Alfvén waves for each run are listed in Table 1.

Figure 1 displays the time evolution of the density fluctuations $\langle(\delta\rho/\rho_0)^2\rangle^{1/2}$ for run 1. It can be found that the evolution has two stages. In the first stage (up to $\varOmega_{\rm p}t \approx 550$), the density fluctuation increases up to $\langle(\delta\rho/\rho_0)^2\rangle^{1/2} \approx 0.08$ immediately, and then nearly remains constant except for some large oscillations. However, at the beginning of the second stage, the density fluctuation begins to increase rapidly until its saturation with $\langle(\delta\rho/\rho_0)^2\rangle^{1/2} \approx 0.2$ at about $\varOmega_{\rm p}t = 800$.

**Table 1.** The simulation parameters for runs 1–3.

| Run | $\beta_{\rm e}$ | $\beta_{\rm p}$ | Wave numbers |
|---|---|---|---|
| 1 | 0.1 | 0.01 | $k_1$=0.209, $k_2$=0.094 |
| 2 | 0.1 | 0.01 | $k_1$=0.136, $k_2$=0.168, $k_3$=0.199, $k_4$=0.230, $k_5$=0.262 |
| 3 | 0.3 | 0.8 | $k_1$=0.209, $k_2$=0.094 |

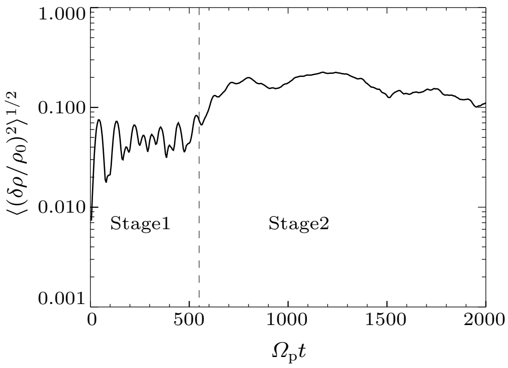


**Fig. 1.** Time evolution of the density fluctuations $\langle(\delta\rho/\rho_0)^2\rangle^{1/2}$ for run 1. The two stages (stage 1 and stage 2) of the time evolution are separated by a vertical dashed line at $\varOmega_{\rm p}t \approx 550$.

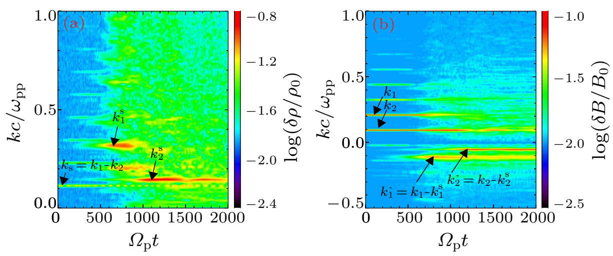


**Fig. 2.** Time evolution of the power spectra for (a) the density fluctuations and (b) the magnetic field fluctuations for run 1. In panel (a) the density modes ($k_{\rm s}$, $k_1^{\rm s}$, and $k_2^{\rm s}$) are denoted by arrows. In panel (b) the pump Alfvén wave modes ($k_1$, $k_2$) and the daughter Alfvén wave modes ($k_1^-$, $k_2^-$) are also denoted by arrows, respectively.

Figure 2 displays the time evolution of the power spectra for the density fluctuations (Fig. 2(a)) and the magnetic field fluctuations (Fig. 2(b)) for run 1. In Fig. 2(a) we can find that in the first stage a density mode with the wave number ($k_{\rm s}c/\omega_{\rm pp} \approx (k_1 - k_2)c/\omega_{\rm pp} \approx 0.115$) appears first, and such a density mode is the result of the envelope modulation of the two incoherent pump Alfvén waves. The higher harmonic density modes with wave numbers $2k_{\rm s}$, $3k_{\rm s}$, and $4k_{\rm s}$ can also be excited. The interactions between these density modes and the pump Alfvén waves lead to the generation of several modes of magnetic fluctuations. This can be demonstrated more clearly in Fig. 3, which plots the power spectra of the density fluctuations (Fig. 3(a)) and the magnetic fluctuations (Fig. 3(b)) at $\Omega_{\rm p}t = 200$ for run 1. To fully understand the coupling processes between the density modes and the Alfvén modes, we have carefully calculated the wave-number relations of all wave modes in the system. The results have also been presented in Fig. 3. The wave numbers of the excited magnetic fluctuations include $(k_2 - k_{\rm s})c/\omega_{\rm pp} \approx -0.021$, which propagates backward, and $(k_1 + k_{\rm s})c/\omega_{\rm pp} \approx 0.324$, $(k_1 + 2k_{\rm s})c/\omega_{\rm pp} \approx 0.439$, etc., which propagate forward.

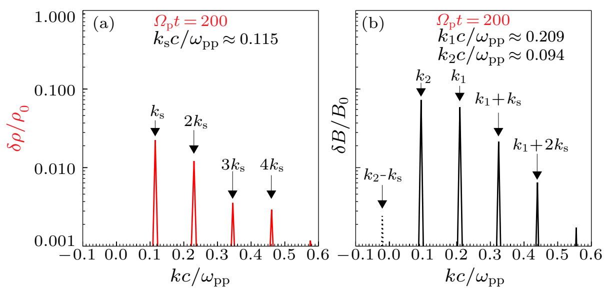


**Fig. 3.** The power spectra of (a) the density fluctuations and (b) the magnetic field fluctuations at $\Omega_{\rm p}t = 200$ for run 1. The black lines and red lines show the magnetic and density fluctuations, respectively. The forward modes and backward modes are denoted by solid lines and dashed lines, respectively. In panel (a) the density mode ($k_{\rm s}$) and its higher harmonic modes ($2k_{\rm s}$, $3k_{\rm s}$, and $4k_{\rm s}$) are denoted by arrows, respectively. In panel (b) the pump Alfvén wave modes ($k_1$, $k_2$) and the daughter Alfvén wave modes ($k_2 - k_{\rm s}$, $k_1 + k_{\rm s}$, and $k_1 + 2k_{\rm s}$) are denoted by arrows, respectively.

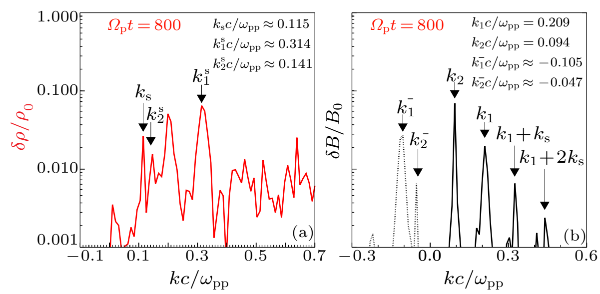


**Fig. 4.** The power spectra of (a) the density fluctuations and (b) the magnetic field fluctuations at $\Omega_{\rm p}t = 800$ for run 1. The black lines and red lines show the magnetic and density fluctuations, respectively. The forward modes and backward modes are denoted by solid lines and dashed lines, respectively. In panel (a) the density modes ($k_{\rm s}$, $k_1^{\rm s}$, and $k_2^{\rm s}$) are denoted by arrows, respectively. In panel (b) the pump Alfvén wave modes ($k_1$, $k_2$), the daughter Alfvén wave modes ($k_1^-$, $k_2^-$, $k_1 + k_{\rm s}$, and $k_1 + 2k_{\rm s}$) are denoted by arrows, respectively.

Figure 4 demonstrates the power spectra of the density fluctuations (Fig. 4(a)) and the magnetic fluctuations (Fig. 4(b)) at $\Omega_{\rm p}t = 800$ for run 1. All the dominant modes and the wave-number relations among them are also provided in both the panels. It is found that, in the second stage, in addition to the residual wave modes excited in the first stage, each pump Alfvén wave will decay into a forward propagating density mode and a backward propagating daughter Alfvén wave. The wave numbers of the density modes corresponding to the pump waves ($k_1c/\omega_{\rm pp} = 0.209$ and $k_2c/\omega_{\rm pp} = 0.094$) are $k_1^{\rm s}c/\omega_{\rm pp} \approx 0.314$ and $k_2^{\rm s}c/\omega_{\rm pp} \approx 0.141$, respectively, while the daughter Alfvén waves have wave numbers $k_1^-c/\omega_{\rm pp} \approx (k_1 - k_1^{\rm s})c/\omega_{\rm pp} \approx -0.105$ and $k_2^-c/\omega_{\rm pp} \approx (k_2 - k_2^{\rm s})c/\omega_{\rm pp} \approx -0.047$. This physical process in the secondary stage can be roughly considered as the superposition of the parametric decay of each pump Alfvén wave.

Figure 5 shows the time evolution of the power spectra for the density fluctuations (Fig. 5(a)) and the magnetic fluctuations (Fig. 5(b)) during the parametric instabilities of five pump Alfvén waves in run 2. Similar to the parametric instabilities of the two pump Alfvén waves in run 1, this evolution can also be divided into two stages. In the first stage, more density modes are excited due to the envelope modulation of the five pump Alfvén waves, and more modes of the magnetic fluctuations are generated due to the interactions between the density modes and the pump Alfvén modes. In the second stage, each pump Alfvén wave can decay into a forward propagating density mode and a backward propagating daughter Alfvén wave mode. Compared with the case of two pump waves in run 1, both the density and magnetic fluctuations show a broader and more continuous spectrum in run 2.

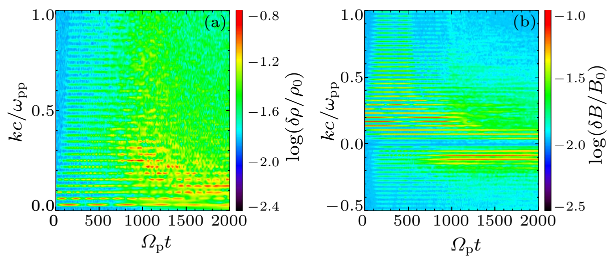


**Fig. 5.** Time evolution of the power spectra for (a) the density fluctuations and (b) the magnetic field fluctuations with five initial pump Alfvén waves for run 2.

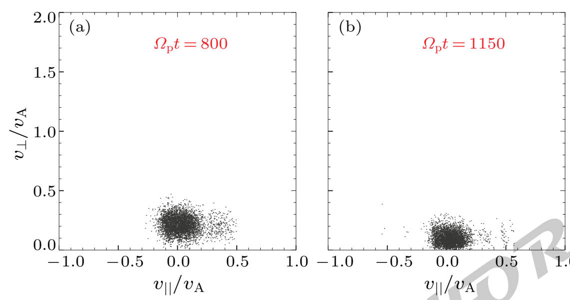


**Fig. 6.** Scatter plots of protons in the $(v_{||}, v_\perp)$ space, panel (a) for run 1 at $\Omega_{\rm p}t = 800$ and panel (b) for run 2 at $\Omega_{\rm p}t = 1150$.

Figure 6 shows the velocity distributions of protons at $\Omega_{\rm p}t = 800$ for run 1 in Fig. 6(a) and at $\Omega_{\rm p}t = 1150$ for run 2 in Fig. 6(b). A proton beam can be observed just after the saturation of parametric instabilities in both runs, which is due to the Landau resonance with the excited ion acoustic waves.

Figure 7 presents the time evolution of the power spectra for the density fluctuations (Fig. 7(a)) and the magnetic fluctuations (Fig. 7(b)) in run 3. As shown in Fig. 7(a), the density fluctuations $k_s$ are also generated rapidly.[37] Then the wave-coupling processes between these density fluctuations and pump waves can be observed in the early stage in Fig. 7(b). However, compared with the results of run 1, the subsequent parametric decay for each pump wave is strongly suppressed (Figs. 7(a) and 7(b)), which may be due to the strong damping of ion acoustic waves in the high beta plasma.

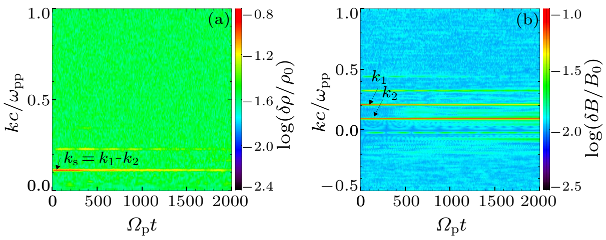


**Fig. 7.** Time evolution of the power spectra for (a) the density fluctuations and (b) the magnetic field fluctuations for run 3. In panel (a) the density mode ($k_s$) is denoted by an arrow. In panel (b) the pump Alfvén wave modes ($k_1$, $k_2$) are also denoted by arrows, respectively.

In summary, by using 1-D hybrid simulations, we have analyzed in detail the parametric instabilities of the pump Alfvén waves with a spectrum in a low beta plasma and found that the evolution has two stages. Before the parametric decay of each pump Alfvén wave, the modulation of the pump Alfvén waves due to spatial inhomogeneity of the magnetic pressure (i.e., ponderomotive force) can cause density fluctuations and their interactions with the pump Alfvén waves can further lead to magnetic fluctuations. Therefore, compared with the monochromatic cases, much more density and magnetic wave modes with a broad spectrum can be generated during the evolution of the parametric instabilities of the Alfvén waves with a spectrum. Moreover, the proton velocity beam will also be formed after the saturation of the parametric instabilities. In the high beta case, due to the strong damping of ion acoustic modes, the parametric decay in the second stage will be strongly suppressed.

## References

[1] Barnes A and Hollweg J V 1974 *J. Geophys. Res.* **79** 2302
[2] Hollweg J V 1974 *J. Geophys. Res.* **79** 1539
[3] Ferraro V C A 1955 *Proc. R. Soc. London* A **223** 310
[4] Mahajan S M and Krishan V 2005 *Mon. Not. R. Astron. Soc.* **359** L27–L29
[5] Galeev A A and Oraevskii V N 1963 *Sov. Phys. Dokl.* **7** 998
[6] Sagdeev R Z and Galeev A S 1969 *Nonlinear Plasma Theory* (New York: Benjamin)
[7] Goldstein M L 1978 *Astrophys. J.* **219** 700
[8] Derby N F 1978 *Astrophys. J.* **224** 1013
[9] Lashmore-Davies C N and Stenflo L 1979 *Plasma Phys.* **21** 735
[10] Ruderman M S and Simpson D 2004 *J. Plasma Phys.* **70** 143
[11] Sakai J I and Sonnerup B U O 1983 *J. Geophys. Res.* **88** 9069
[12] Longtin M and Sonnerup B U O 1986 *J. Geophys. Res.* **91** 6816
[13] Wong H K and Goldstein M L 1986 *J. Geophys. Res.* **91** 5617
[14] Terasawa T, Hoshino M, Sakai J I and Hada T 1986 *J. Geophys. Res.* **91** 4171
[15] Hoshino M and Goldstein M L 1989 *Phys. Fluids* B **1** 1405
[16] Jayanti V and Hollweg J V 1993 *J. Geophys. Res.* **98** 19049
[17] Hollweg J V, Esser R and Jayanti V 1993 *J. Geophys. Res.* **98** 3491
[18] Hollweg J V 1994 *J. Geophys. Res.* **99** 23431
[19] Araneda J A 1998 *Phys. Scr.* **T75** 164
[20] Del Zanna L, Velli M and Londrillo P 2001 *Astron. Astrophys.* **367** 705
[21] Araneda J A, Marsch E and Vinas A F 2007 *J. Geophys. Res.* **112** A04104
[22] Zhao J S, Voitenko Y, Wu D J and De Keyser J 2014 *Astrophys. J.* **785** 139
[23] Zhao J S, Voitenko Y, De Keyser J and Wu D J 2015 *Astrophys. J.* **799** 222
[24] Vinas A F and Goldstein M L 1991 *J. Plasma Phys.* **46** 129
[25] Nariyuki Y and Hada T 2007 *J. Geophys. Res.* **112** A10107
[26] Nariyuki Y, Hada T and Tsubouchi K 2007 *Phys. Plasmas* **14** 122110
[27] Kauffmann K and Araneda J A 2008 *Phys. Plasmas* **15** 062106
[28] Matteini L, Landi S, Del Zanna L, Velli M and Hellinger P 2010 *Geophys. Res. Lett.* **37** L20101
[29] Verscharen D, Marsch E, Motschmann U and Muller J 2012 *Phys. Rev.* E **86** 027401
[30] Gao X L, Lu Q M, Li X, Shan L C and Wang S 2013 *Phys. Plasmas* **20** 072902
[31] Nariyuki Y, Hada T and Tsubouchi K 2014 *Astrophys. J.* **793** 138
[32] Bruno R and Carbone V 2013 *Living Rev. Sol. Phys.* **10** 2
[33] Tu C Y and Marsch E 1995 *Space Sci. Rev.* **73** 1
[34] Narita Y, Glassmeier K H and Treumann R A 2006 *Phys. Rev. Lett.* **97** 191101
[35] Verscharen D, Marsch E, Motschmann U and Muller J 2013 *Phys. Plasmas* **20** 022305
[36] Howes G G 2015 *Philos. Trans. R. Soc.* A **373** 20140145
[37] Matteini L, Landi S, Velli M and Hellinger P 2010 *J. Geophys. Res.* **115** A09106
[38] Winske D 1985 *Space Sci. Rev.* **42** 53
[39] Quest K B 1988 *J. Geophys. Res.* **93** 9649
[40] Winske D and Omidi N 1993 *Computer Space Plasma Physics: Simulation Techniques and Software* (Tokyo: Terra Science Publishers)

# Chinese Physics Letters

**Volume 32 Number 11 November 2015**